ENGR7019 MSc Engineering Dissertation Final Report

Impacts of Fluid Structure Interaction on Formula Student Front Wing

Myles Ginty - 19217127

Programme:	Motorsports Engineering
Module:	ENGR7019: MSc Dissertation
Academic year:	2024-2025

School of Engineering, Computing and Mathematics

Abstract

Aerodynamics is critical to motorsport design and yet many studies of fluid flow analysis use static geometry, overlooking how the aerodynamic loads and structural deformations interact. By performing this Fluid-Structure coupled simulation, it provides a more realistic understanding of fluid changes in a dynamic scenario.

This analysis investigates the integration of Computational Fluid Dynamics (CFD) with solid stress validation into another level of concurrent-type simulations. To evaluate Fluid flow, CFD is used to simulate the flow by computing mathematical models to represent the turbulent flow over a given design. Since standard CFD has static geometry, by having the geometry change with the computed loads over time provides a more accurate representation of fluid flow analysis. This study of a 2025 Formula Student Front wing will aim to quantify the interaction of aerodynamic load and deflection impact on lift and drag.

By starting with an initial simplified design to develop both CFD in Steady and Unsteady models before moving to an FSI validation, the simulation functionality using the k-omega model is demonstrated. Subsequently, migration to a full wing design with accurate materials provided a thorough analysis of designs, it illustrated the benefit of executing more accurate simulations. This 2025 design uses the accurate composite properties in a Fluid Structure Interaction analysis to evaluate the deformation, aerodynamic forces and flow characteristics.

The results reported in this analysis show a difference in deflection, lift and drag at various ride heights, with improvement in the pitching configuration. Other outputs to illustrate the impact of this methodology include flow velocity and surface pressure combined with the corresponding wing deflection, providing additional explanation to the change in the wing performance. While there is a difference in the front wing performance when the wing is deflected, it is not as impactful as altering the pitching geometry as the difference in rotation is ten times that of the deflection of the wing itself. These findings highlight the importance of incorporating FSI methodology into standard aerodynamic design optimisation.

Table of Contents

Illustrations

List of Figures

List of Tables

Introduction

To validate a design in the field of Fluid Dynamics, there are many methods that can help illustrate the performance benefits. While there are many levels of simulations that will sufficiently illustrate Fluid Dynamics, the design itself does not change transiently with most simulations. To allow an aerodynamic device to change with the transient flow, Fluid Structure Interaction (FSI) must be performed. By performing this analysis on a Formula Student Front wing, there is a clear listing of the materials used, providing an accurate representation of the aerodynamic and structural validation with this design, which would otherwise be inaccessibly confidential in a higher-performance series front wing. The objective of this analysis is to establish a baseline design and materials, which is then used to develop the steady state and transient CFD. This will be compared with the baseline Fluid Structural Interaction simulation, which will then validate the versatility of the design in various ride heights. While Fluid Structural Interaction analysis is applicable to any vehicle aerodynamic device, the impact of the deflection would be most visible with the front wing due to its proximity to the ground plane and boundary layer. This exploration of the change in front wing heights, further supports the exploration with conventional testing methodology of ride heights with aero maps.

Objective

The primary aim for this study is to provide a demonstration of performance differences between a FSI and a standard CFD analysis to provide a more accurate level of performance of a Formula Student front wing design. The objective of this analysis is to model and simulate a simplified wing, then a full Formula Student Front wing device, encompassing the investigation of different loading conditions and monitoring the subsequent structural deformations.

Background

For designs to be validated aerodynamically, numerical modelling softwares are used to compute the fluid flow using different expressions to evaluate areas of the design. A typical evaluation of a vehicle's aerodynamics in simulation uses a numerical modelling technique called Computational Fluid Dynamics (CFD) in a steady state condition. Using specialised software to solve the flow of particles through a domain and over a body to help provide the forces on the body and evaluate what to expect for an effective design, in this instance, to provide vertical force to increase traction of the vehicle. However, depending on the setup, a CFD can be limited in its evaluation, only providing forces and an illustration of flow and not seeing how those forces could change the structure in real-time. While an FSI Model computes the aerodynamic performance transiently and mimics the aeroelastic effect on devices (Gong and Zhang, 2019). Fluid-structural interactions add material properties to show not only the forces on the body but also how the forces change the body, impacting the flow, further changing the simulation results (Patil et al., 2015). Since an FSI model is a more evolved and a more direct representation of fluid flow than that of a fixed geometry CFD model, further examination can be done to prove the change in performance with changing load conditions by exploring different vehicle ride heights.

Literature Review

There are several aspects to the experimentation of Fluid Structure Interaction (FSI) that have already been achieved. Referencing this literature will allow for not only avenues of project methodology but also to find relevant published materials to review and evaluate

for topics in Geometry, CFD, FSI as well as the input and outputs of the required analysis. The review of these included topics required to construct a successful simulation will help refine and establish a baseline model to validate the selected designs.

Airfoil geometry

While the ideal comparison would be on a Formula 1 design due to the operating speeds and forces that illustrate aeroelasticity, (Bang, C.S. et al., 2022) the construction, properties and resources are not regularly available to the public. While there are experiments performed on formula student designs, they have not been evaluated to this level in a Fluid Structural Interaction simulation. Since the the wing properties are known, this makes the simulation a more accurate choice of evaluation.

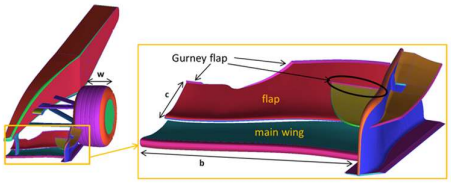

Figure 1: Formula 1 Front wing Geometry (Mattia Basso, Carlo Cravero and Davide Marsano, 2021)

Some aspects worth considering for the FS front wing design, is how the front wing will interact with the nosecone (Rangarajan et al., 2025). This will be a factor as the trailing edge and upper surface towards the centre of the wing is impacted by this design. By decreasing the angle of attack and positioning, an optimum front wing can be designed to match the high energy caused by the draft of the nosecone (Karthikeyan and Radhakrishnan, 2024). A notable design feature added to wings is the addition of a gurney flap on the trailing edge of the flaps to promote attachment of the flow. A 30% increase in overall performance has been shown when the gurney flap is added (Mattia Basso, Carlo Cravero and Davide Marsano, 2021). One of the drawbacks on gurney flaps is the impact on aero devices behind the gurney flaps, as it creates a distorted wash on devices behind the wing, such as the floor as seen in Figure 1 (Mattia Basso, Carlo Cravero and Davide Marsano, 2021). While the full flap design will provide the best results, to test and construct a functional simulation, a simplified design will be needed to evaluate the complexity before the refinement and expansion of the simulations with a full wing design.

Computational Fluid Dynamics (CFD)

There are many examples of CFD simulation methods, but not all of them are best suited to an FSI simulation. Some are better for focusing on CFD alone to demonstrate basic directional flow. To perform simulations, equation models need to be selected to compute the conditions of the air particles in the field. Some research explores simplified models in ANSYS using a two-coupling steady-state model (Bang et al., 2022). A common method used particularly in full car simulations for Formula Student is with a steady-state solver using Reynolds-averaged Navier Stokes (RANS) equation models (Zhang et al., 2024). In part this is as a result of the averaged results for each of the computed cells, making it less computationally expensive. While migrating to use an Unsteady Reynolds Average Navier Stokes (URANS) solving model, there will be a better reflection on the effects of the airfoil by seeing the flow change with time (Brockmeyer et al., 2024). However, due to this computational expense, with unsteady and is more difficult to produce results it is therefore less common, but very good for monitoring change positioning relative to the ground over time to find the change in performance, making it ideal for an FSI simulation.

Other research done for the construction of front wing design, particularly for Formula 1 front wings, compares the differences between implicit and explicit Large Eddies Simulation (LES) (Ntoukas et al., 2025). This method provides a clearer illustration of the conserved energy produced by large formations, but too complex for FSI. While many CFD simulations typically use RANS, the most straightforward of computations, other URANS solvers are required for FSI

simulations, which enables a detailed illustration of the flow and models with time, allowing for more wake development.

Similar to CFD, the meshing operation is also used with FSI to evaluate the flow and forces on and around the geometry, which measures outputs such as the pressure on the surface of the model or Wall Y+ values as seen in Figure 2. Optimising the mesh quality for this model is a trade-off between minimising computing time and provide accurate results where it matters (Bang, C.S. et al., 2022). With each timestep of the FSI simulation, the mesh then needs to be updated to provide the deflection-updated wing location (Bang, C.S. et al., 2022). This means that the difference between a normal CFD Simulation and one with FSI means the addition of another tetrahedral mesh used for the stress analysis of the device.

Fluid-Structure Interaction

Fluid Structure Interaction (FSI) combines the sequential manner of CFD and Finite Element Analysis (FEA) in an effective and efficient way to find the deflection of the aerodynamic devices caused by the aerodynamic loads. When compared to traditional CFD models with a rigid model, FSI is capable of deformation and updating the conditions of the model for re-evaluation (Ratzel and Dias, 2014). Many other resources have explored the Fluid structural interaction topic with varying levels of validation. Most evaluations are among airfoils but with different independent variables, such as environmental conditions or fluid solver methods (Ghaedi et al., 2021). The level of varying simulation boundary conditions also allows for exploring different strategies with the validation of alternative designs. While this simulation process for Fluid Structural Interaction is typically computationally expensive, to save on simulation time similar to CFD, the typical method is to perform validation on only a half car using a symmetry plane (Shaalan, A. et al., 2024).

There are various softwares that execute both operations separately, but an important factor remains with selecting ones that incorporate FSI with many tools to use for specifying material properties. Some

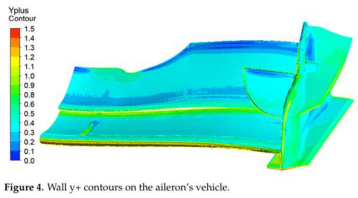

Figure 4. Wall y+ contours on the aileron's vehicle.

Figure 2: Front wing Wall Y+ CFD Contours (Mattia Basso, Carlo Cravero and Davide Marsano, 2021)

softwares often utilise multiple solvers to computing the structural and fluid flow separately in a single simulation in order to add a wider range of materials specifications for the solid stress and fluid flow solvers. AcuSolve uses RADIOSS to solve Fluid Structural Interaction, however, since this is a nonlinear scenario, multiple solvers are often required (Jaiman, Thomas and Shakib, 2012). For Star CCM+ to solve FSI simulations, the software uses a Lagrangian formulation to solve for the Finite Element Method (FEM) displacement while using a separate set of solvers to solve for the Fluid effects (Fuentes, Cura Hochbaum and Schulze, 2023). It is crucial that the software used is not only capable in performing both stress and fluid operations simultaneously but also has a wide variety of material properties to specify whether it is anisotropic or orthotropic materials, allowing for accurate representation for a design's structure (Khayyer, A. et al., 2022). Using a software which supports this, such as Star CCM+, shows the versatility of applications available for fluid structure interaction capabilities for correlating CFD performance validation.

Loading Conditions

To evaluate the vehicle's aerodynamics means addressing where the forces are generated which impact the structure of the design. The loads this wing experiences will vary with the vehicle's position in space for a given speed, which means exploring how adaptable a design is by producing a map of different pitching angles or ride height

variations (Zhang et al., 2024). This change in ride height can be explored and compared in both CFD and FSI-type simulations to see performance differences.

One of the reasons it is important to monitor the deflection change under aero loading is due to the porpoising phenomenon caused by clearance changes. On a vehicle level, when suspension deflection is too great, causing lower ground clearance, it increases the aero performance of the front wing. This causes greater deflection until the wing stalls and rebounds (Marco Gadola et al., 2022). This is why it is important to make sure the structure of the wing is stiff enough to overcome this phenomenon. The best way to monitor the sensitivity to this effect is with Aero Map analysis defined by the corresponding Front and rear axle height, which has an increased effect on the downforce the closer the vehicle is to the ground (Roberts et al., 2016). Since it has the potential to stall in this scenario, it is important to simulate it for various dynamic conditions to examine the versatility of the wing design.

Results

The measure of success will be determined through the evaluation of parameters such as the Coefficient Lift and Drag (CL and CD) as well as structural dependency such as deflection. CL and CD are also valuable to compare over a surface, illustrating how effective an airfoil is over a given space known as Coefficient Drag Area (CDA) and Coefficient Lift Area (CLA). Comparing these two will also provide the efficiency of the airfoil. This presents the impact of shape since the front wing's performance relative to the ground is dependent on the restricted flow between the suction surface and the ground plane as well as the vortices induced by the endplates (Roberts et al., 2016). These forces will be pushing the wing downwards, decreasing the gap, and increasing the wing's performance.

While choosing FSI analysis concludes that there are several aspects to consider. Since CFD, is widely covered, it provides numerous resources to help develop and illustrate new visible areas of FSI Simulations. Executing this analysis with accurate materials and applications, on a Formula Student front wing in Star CCM+, will help to quantitatively explore the differences in the vehicle's performance.

Methodology

Model Development

Like some of the previous FSI explored, such as Fuentes, Cura Hochbaum and Schulze, 2023 the method of these simulations will be similar, first utilising steady state coupled flow CFD before moving to unsteady and adding Solid stress properties to the simulation. Star CCM+ will be used to combine the two present physics, calculating the total Lagrangian displacement while changing in the flow boundary, thus changing the aerodynamic properties (Fuentes, Cura Hochbaum and Schulze, 2023). In Figure 3, a domain with the following geometry was developed for both CFD and FSI simulations based on standard vehicle domain construction recommended by Siemens, with the initial boundary conditions listed in Table 1.

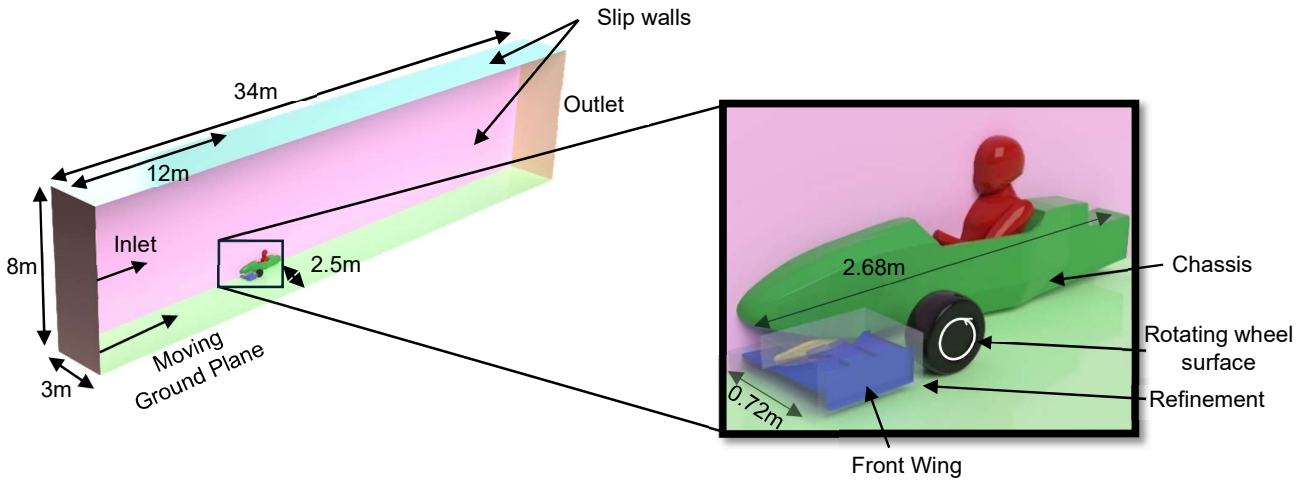

Figure 3: Fluid Structure Interaction Simulation Schematic

For running the initial CFD in an unsteady state and afterwards in a Fluid-Structure Interaction. The simulation needs to be performed using a certain number of iterations before converging on a load to morph a new geometry for each time step recorded. This setup was done in a separate study during development to compare the level of residuals converged. The amount of time past for each step and in the fewest number of iterations to compute would allow for a smooth evaluation of the front wing. This was settled with a physical timestep of 0.05sec for every 30 inner iterations.

Initial Condition Parameters	Target
Inlet speed/ground speed (m/s)	15
Wheel rotation speed (RPM)	735.3
Air Density (kg/m^3)	1.18
Turbulent velocity scale(m/s)	1
Turbulence Intensity	0.01

Table 1: Model Initial Conditions

K-Omega Turbulence Model

The selected turbulence model, k-omega, is used in this analysis for it is an accurate representation of the eddies and flow separation. This maintains an important aspect to this analysis, knowing precisely when the wing forces change, altering the wing's deflection. Based on the mesh sizing, this turbulence model is computed using variables such as the turbulent kinetic energy and dissipation rate. This turbulence model is represented in equations (1) and (2) of the appendices.

FSI Exploration

Geometry Differences

The initial simplified geometry as a proof of concept is shown in Figure 4, which was later swapped with the full wing design as seen, to avoid any conflicts with the initial setup. Following the initial coupled flow Steady/Unsteady CFD and FSI simulations, the full FS Wing geometry was updated with a more representative laminate in order to perform the later following 9 simulations with the aero map varying the ride height by 10mm on the front and rear axles. The main differences in Figure 4 include the simplified cantilever flaps; similarly, the mainplane is only supported by the symmetry plane, whereas the full wing will be supported by the mounting arms connected to the chassis.

(A)

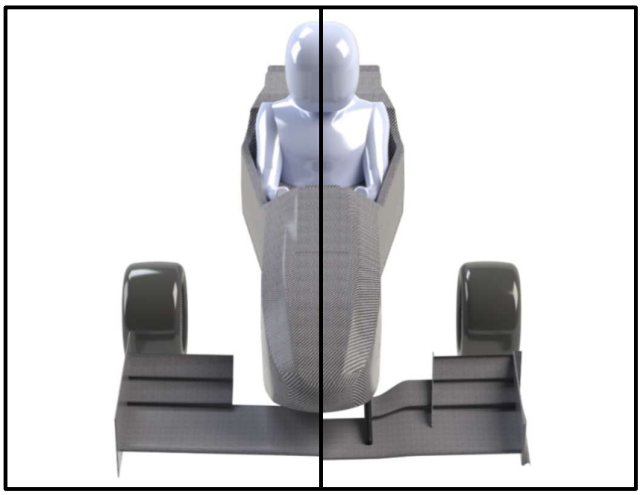

(B)

Figure 4: Formula Student Oxford Brookes Racing 2025 (A) Simplified Wing & (B) Full Front Wing

Material Analysis

In order to assign the solid mesh required for performing the solid stress analysis portion of the Fluid Structure Interaction simulation, properties need to be assigned to replicate the structure of the Front wing design. Due to the basic settings available for Fluid Structure Interaction in Star CCM+, orientation as well as ply quantity is not available, which means alternative simplifying measures need to be taken place. Two methods were used in this instance, with the first assigning both simplified and full FS wing designs as an isotropic material, and the second using a cumulative orthotropic material formulated by a cumulative laminate analysis, instead accurate to the OBR25 Front wing.

(A)

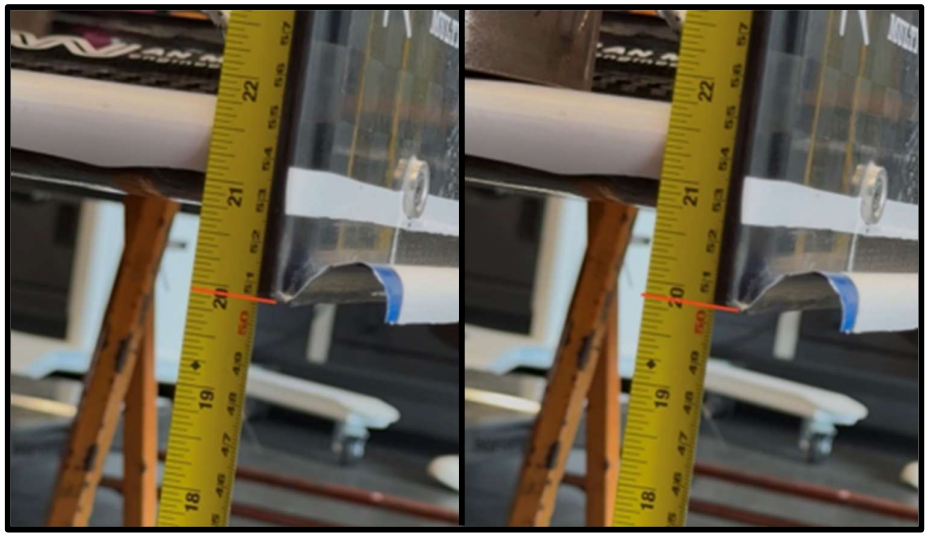

(B)

Figure 5: 200N Front wing deflection test (A) Before & (B) After

The deflection test shown in Figure 5 illustrates the benchmark on which the simulation can reference for the stiffness of the front wing construction. As seen, the wing only deflects about 2mm under a 200N load. While the wing during this simulation should not experience this level of stress, it does allow for a level of comparison to the simulation results.

Initial Isotropic Composite

For a proof of concept, an initial set of properties was required of laminate materials in place of what was used on the FS front wing design. Selecting the results of an Oxford Brookes

Racing test specimen shown in Figure 6. Although the laminate materials differ from the 2025 design, they use a comparable number of plies and orientation sequence; this particular specimen was chosen to accurately represent the wing's properties to prove the functioning simulation.

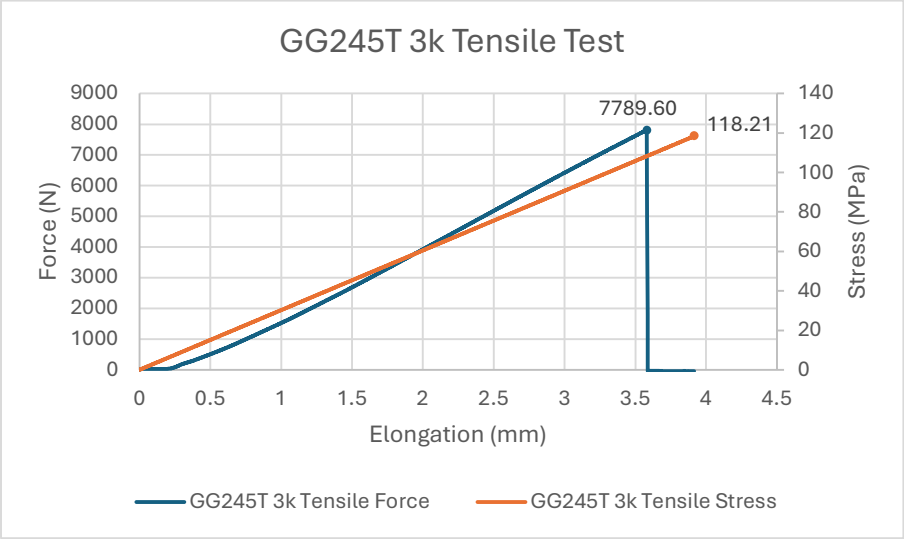

Figure 6: GG245T test specimen implemented for properties

Cumulative Equivalent Laminate Composite

For the final analysis and aero map, the simulations required an equivalent laminate analysis to assign the assumed laminate for the front wing. While this wing's design used an internal wing design to improve the structure. This analysis will take the wing from the perspective of a worst-case scenario, not including the internal structure for a less complex model. The laminate sequence used spread-tow at 0/90°, then a layer of 45° T800, followed by another layer of spread-tow. The listed from Equations 1-10 were used to calculate the equivalent laminate properties for the final set of simulations, where Q is the composite Stiffness, E is Young's Modulus, G is Shear Modulus and v is Poisson's ratio in the directions illustrated in Table 2.

Equations

$$Q_{11} = \frac{E_{11}}{(1 - v_{12}v_{21})} \quad (1)$$

$$Q_{22} = \frac{E_{22}}{(1 - v_{12}v_{21})} \quad (2)$$

$$Q_{12} = \frac{v_{21}E_{11}}{(1 - v_{12}v_{21})} = \frac{v_{21}E_{22}}{(1 - v_{12}v_{21})} \quad (3)$$

Equation 1: Stiffness Equations

$$A_{ij} = \sum_{k=1}^{n} \left(\overline{Q_{ij}}\right)(z_k - z_{k-1}) \quad (4)$$

$$E_{xx} = \frac{1}{tA_{11}} \quad (5)$$

$$B_{ij} = \frac{1}{2}\sum_{k=1}^{n} \left(\overline{Q_{ij}}\right)({z_k}^2 - {z_{k-1}}^2) \quad (6)$$

$$E_{yy} = \frac{1}{tA_{22}} \quad (7)$$

$$G_{xy} = \frac{1}{tA_{66}} \quad (8)$$

$$(9)$$

$$D_{ij} = \frac{1}{3}\sum_{k=1}^{n}\left(\overline{Q_{ij}}\right)\left({z_k}^3 - {z_{k-1}}^3\right)$$

Equation 2: Transformed Stiffness equations

$$v_{xy} = -\frac{A_{12}}{A_{11}} \quad (10)$$

Equation 3: Laminate Membrane Equations

Using the previous equations, the following calculated properties in Table 2 were collected to be evaluated as an Orthotropic material in the final fluid structure interaction simulation and Aero map.

Material Properties		Unidirectional T800	Spread Tow Target	Equivalent Laminate (Orthotropic)	Testing 3 ply laminate (Isotropic)	Material Properties Orientation
Young's Modulus (MPa)	E1	137000	55200	60400	11467.33	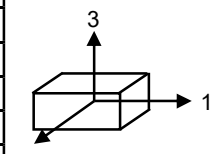
	E2	8100	55200	60400	11467.33	
Poisson Ratio		0.33	0.05	0.065	0.33	
Shear Modulus (MPa)	G12	3760	2900	3520	N/A	
	G13	2506	2500	506	N/A	
	G23	2506	2500	506	N/A	
Thickness (mm)		0.1527	0.12	0.3927	N/A	

Table 2: Composites Properties used for Solid stress analysis

Model Development

The flow chart in Figure 7 shows the process for constructing the required simulations to validate the Formula Student front wing design. First, the baseline concept for the standard CFD simulations for Steady and Unsteady state conditions to run for the simplified wing, then FS front wing was developed. After this concept phase, the simplified wing would be used to help develop the FSI simulation before moving to the full wing design. At the same time, updating the laminate properties for the FS front wing design, a more representative orthotropic laminate was used to evaluate the final aero map.

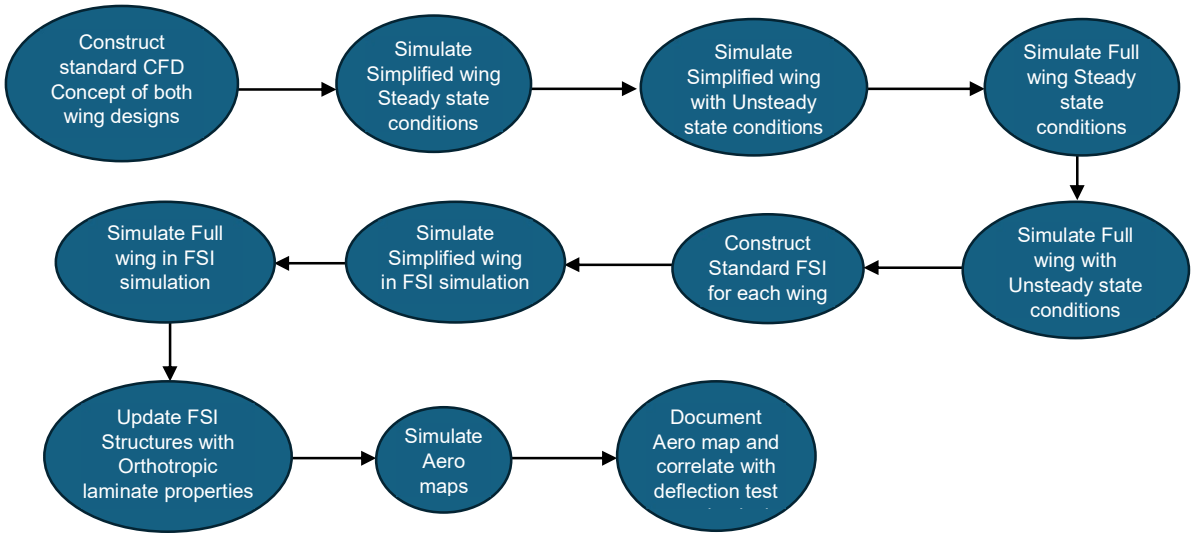

Figure 7: Simulation Model development process

Meshing

To accurately represent the geometry in the simulation, different meshes are required. The solid and fluid meshes were then connected by an interface to transfer the loads between the fluid flow and solid stress analysis. The fluid mesh used in this analysis, as shown in Figure 8, is comprised of a trimmed cell mesh with a minimum size of 10 mm and a total number of 18.25 million cells, as seen in Table 3. While in the standard CFD phase of this model, a more accurate polyhedral mesh using 15 million cells was used to accurately represent the geometry. A trimmed cell approach is only available for a Fluid Structure Interaction simulation setup in the Star CCM+ software.

Using the same geometry and domain, many of the mesh settings remain the same as the design analysis performed with Oxford Brookes Racing; as a result, this analysis will not include a mesh convergence study, as this is not the focus of this study. The selected mesh for the solid stress validation, however, was selected in accordance with the standard suggested procedure of the Star CCM+.

	Fluid Mesh			Solid Mesh
	CFD RANS	CFD URANS	FSI Fluid	Front wing
Cell type	Polyhedral	Polyhedral	Trimmed Cell	Tetrahedral
Base size	50	50mm	100mm	5mm
Target size	5mm	50mm	50mm	5mm
Minimum Surface Size	0.5mm	0.5mm	10mm	0.5mm
Surface Curvature	200pts/circle	200pts/circle	36pts/circle	36pts/circle
Cell count	14.94 million	15.14 million	18.25 million	2.642 million

Table 3: Simulation Mesh sizing

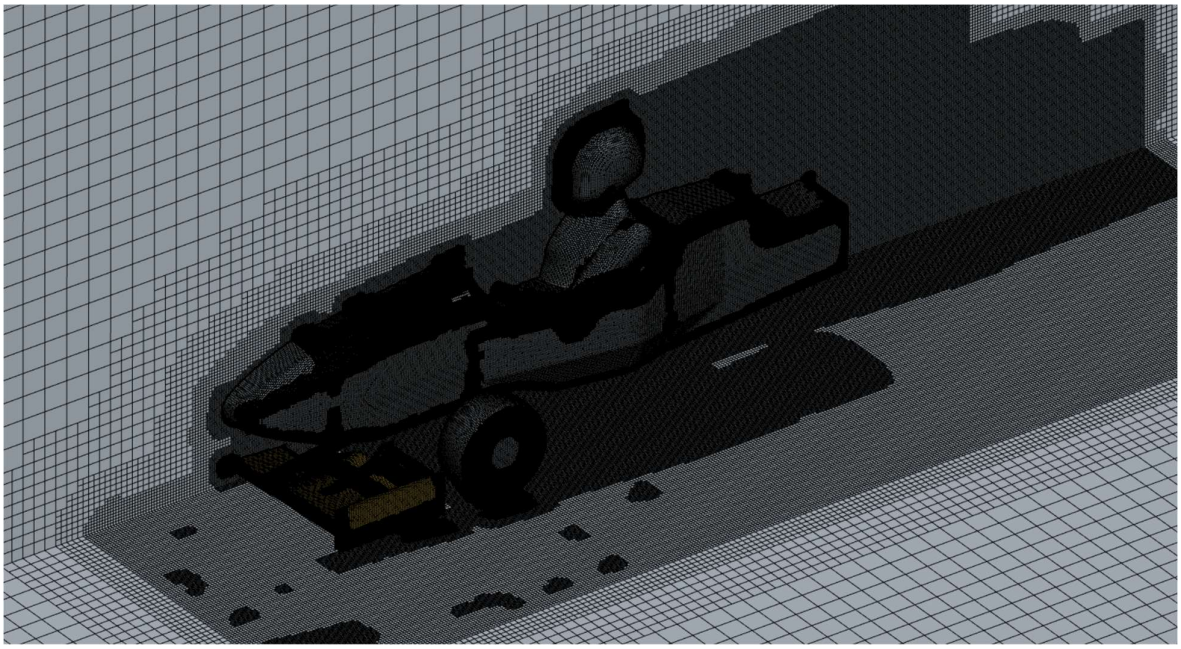

Figure 8: Fluid Domain Mesh

The solid mesh, as seen in Figure 9, used to perform the stress analysis of these FSI simulations. A tetrahedral cell mesh is applied to the wing surface with a total number of 2.642 million cells and a minimum cell size of 0.5mm for the wing as listed in Table 3. These two sets of meshes are linked by an interface so that the changes in surface pressures from the fluid flow can be applied to the surface of the solid mesh to update the displacement.

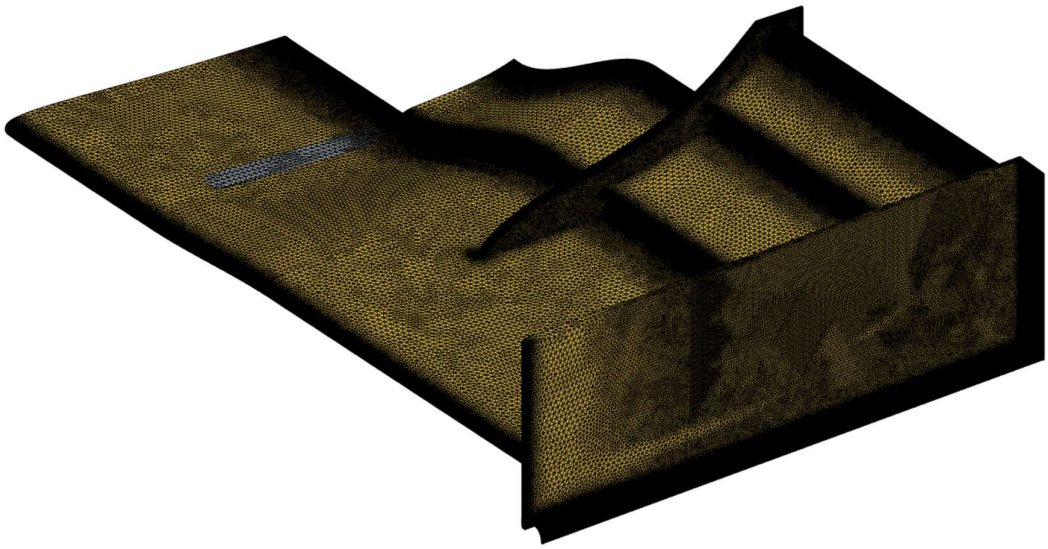

Figure 9: Full Wing Solid Mesh

While other simulation softwares are able to assign the laminate in order of plies, by using an orthotropic material with this solid mesh assumes orientation relative to the physical geometry. The properties of the laminate as seen in Table 2 have been computed to represent the strength in the specified orientation; however, this remains applicable since the application of the properties is in the same global coordinate system.

To conclude a thorough validation of the front wing design the following simulations listed in Table 4 were performed first to verify the simulation using a simplified then full FS wing design before pursuing the aero map. This means a total of 12 FSI simulations and 4 standard URANS and RANS CFDs were executed to validate this design.

Sim #	Turbulence Model	Material Properties	Geometry	RH (FRH x RRH)
1	RANS	Isotropic	Simplified model	35 x 35
2			Full FS wing model	
3	URANS		Simplified model	
4			Full FS wing model	
5	FSI/URANS		Simplified model	
6			Full FS wing model	
7	FSI/URANS	Orthotropic	Full FS wing with Updated Equivalent composites	
8	FSI/URANS	Orthotropic	Aero Map	20 x 20
9				20 x 30
10				20 x 40
11				30 x 20
12				30 x 30
13				30 x 40
14				40 x 20
15				40 x 30
16				40 x 40

Table 4: List of Front wing simulations and corresponding ride heights for each cell

Constraints

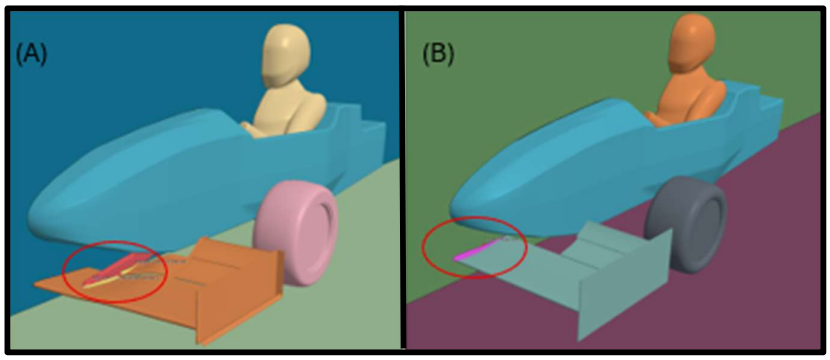

Figure 10: FSI Support interfaces Full Front Wing support interfaces (A) FS Full Front wing & (B) Simplified Wing

To restrain the wing, constraints were used to develop the Fluid Structure Interaction model and are illustrated in Figure 10. While there are some differences in the hardware that would be used on the physical wing. The full wing does have the correct localised support to the mainplane and first flap. For a simplified representation, a cantilever support to the mainplane was successfully tested before migrating to the full wing.

Results and Discussion

Steady vs Unsteady CFD

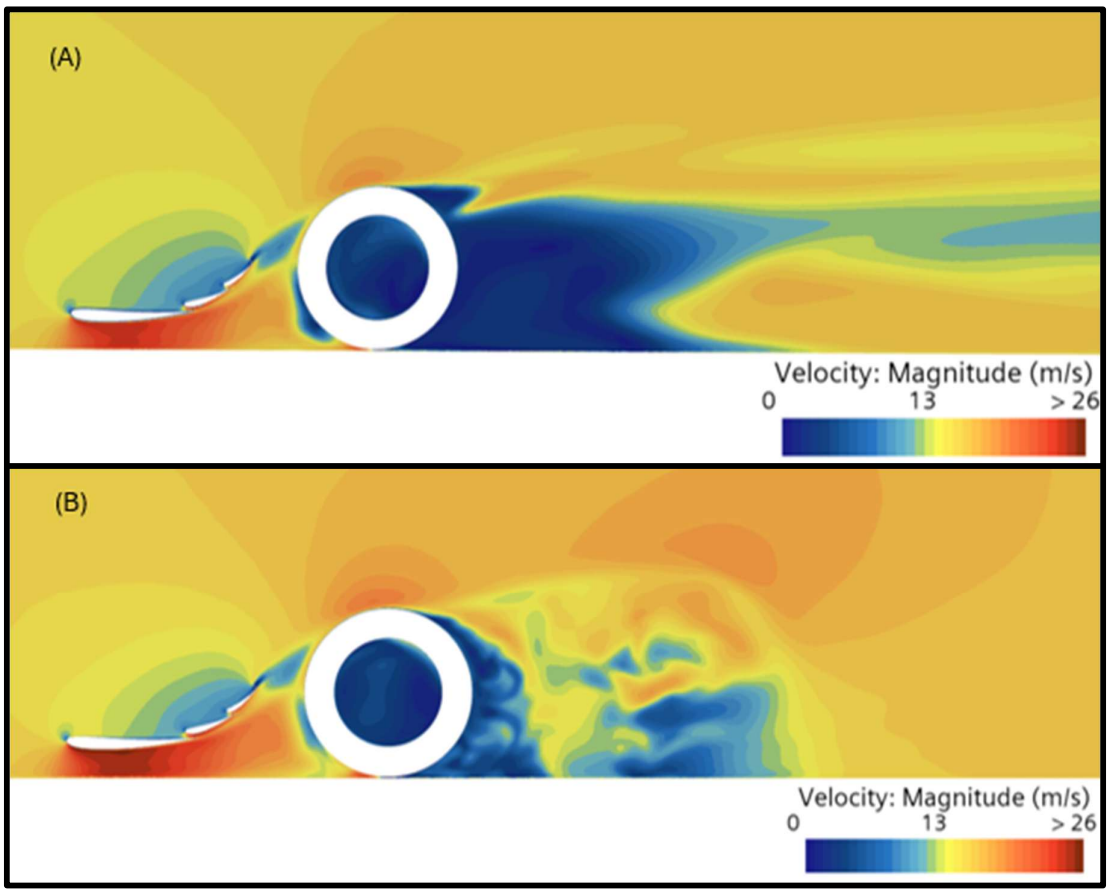

Figure 11: Velocity scalar 0.55m from the centre of Full Front Wing in (A) RANS and (B) URANS simulation

In the comparison in Figure 11, the benefits of evaluating in Unsteady conditions using the k-omega solver are presented. A visual representation of the eddy formations in the wake region is shown, which are often overlooked in the Steady-state model. The unsteady results still show similarities to the RANS simulation trailing edge regions and around the front wing itself, which indicates a consistent representation to explore FSI next.

CL and CD Geometry Comparison

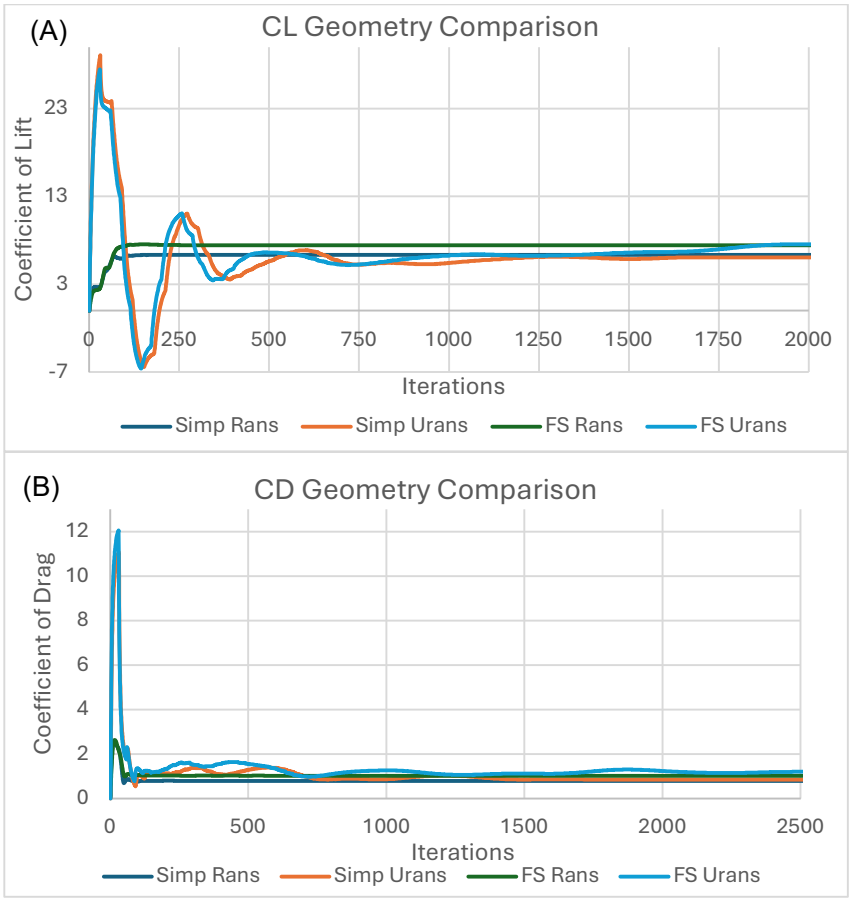

Figure 12: Geometry Comparison of Simplified and FS Full Front Wing Designs (A) CL & (B) CD

The comparison between these geometries and the simulation type provides a difference in some aspects of performance. For example, in Figure 12, the Simplified model achieves a lower CL in an unsteady scenario a bit sooner than the FS Full wing; however, the noticeable difference is how quickly a steady state model converges with both designs.

FSI Exploration

Isotropic Simplified vs Full Wing

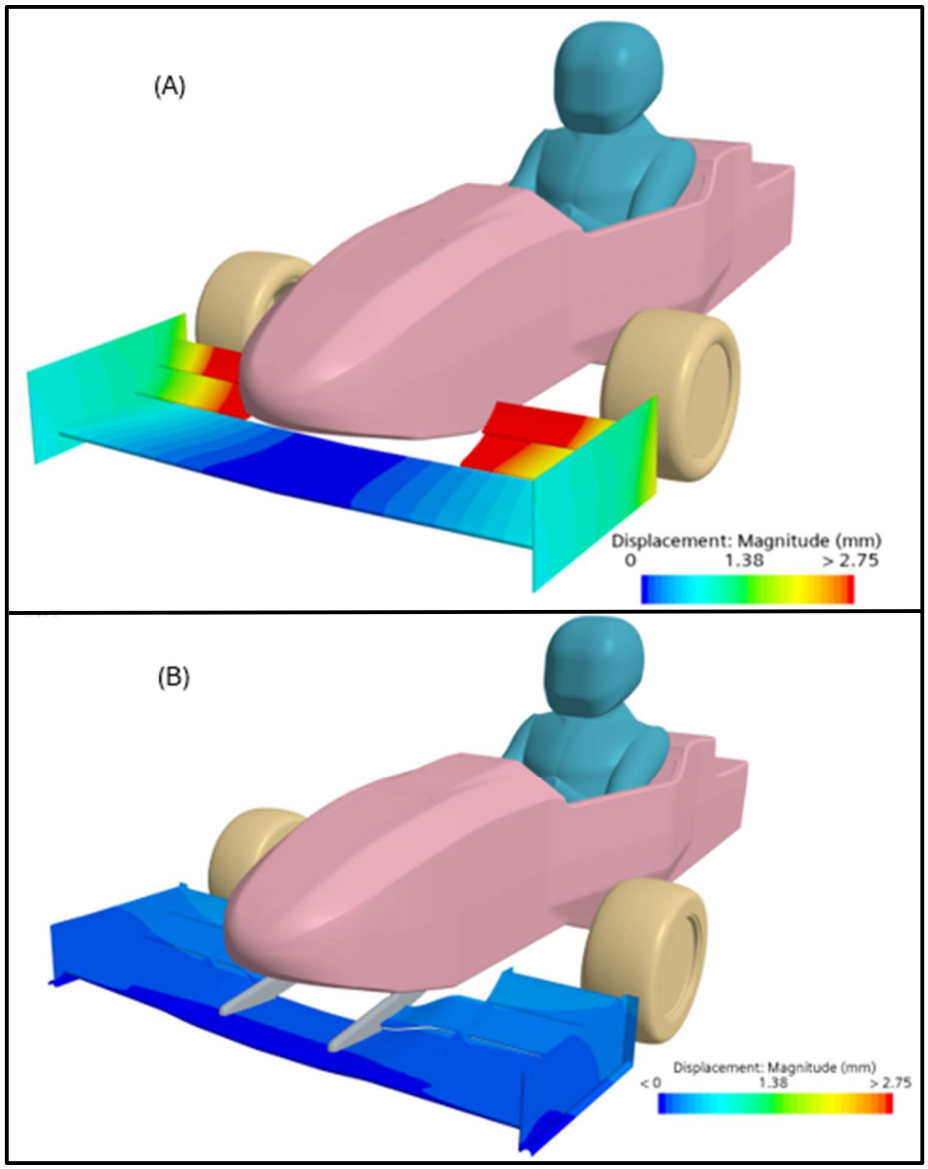

Figure 13: Isotropic FSI Simulations (A) Simplified Front Wing & (B) FS Full Front Wing

The first analysis of the Formula Student Front wing was executed using a simplified model. By using the simplified wing along with the Isotropic material properties listed in Table 2. An initial simulation illustrated the model's functionality before migrating to the full wing design in Figure 13, showing the difference in deflection caused by the different construction. The isotropic simplified and FS full wing was observed to be significantly closer to the inside of the upper flaps, indicating the impact that the vertical load has on these simplified properties. The magnitude of deflection was also noticeably greater on the unsupported flaps of the simplified model.

Furthermore, while the focus in the Isotropic simulations is on the flaps, the contrary is later shown with the Orthotropic, migrating the maximum deflection towards the endplates shown in Figure 18. This presents a more realistic approach to the front wing deflection. Since both

initial models have the same test specimen properties as listed in Table 2, the likelihood for the differentiation in the results shown in Figure 13 is due to the physical construction of the design and the support at which the front wing is constrained. Where the simplified model uses cantilevered upper flaps and a cantilevered mainplane, the FS Full wing is supported by the first flap and the mainplane, with the upper flaps supported by the midplates providing a much stronger assembly.

Formula Student Full Wing with Orthotropic Composites

Transient Simulation recordings 35-35 Ride-height

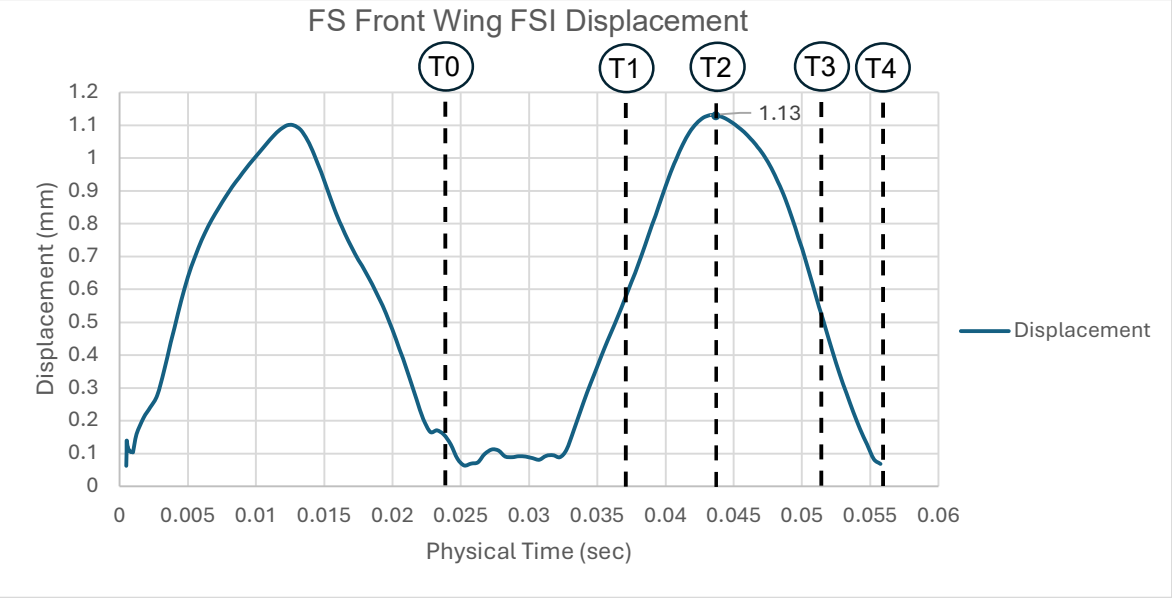

Figure 14: Displacement VS time at 35-35 ride height

Figure 14 shows the oscillation present in the wing's deflection. Listed in Table 5 is the wing's performance at various intervals following the FSI simulation convergence on a force applied to the front wing, which occurs at T0. After this point, the force applied to the wing is relatively constant +/-10% where the simulation converges and then reaches maximum deflection at T2. After this, either a period of separation or spring back from the natural undamped resistance properties to permanent deflection of pure carbon fibre caused the front wing to rebound as seen.

Should there be a point of separation, however, this would have been noticeable in the forces in Figure 15. After the convergence, the net force of the front wing remains consistent. Since this simulation is recorded over a short period, the oscillation is more likely due to the lack of natural damping by the carbon fibre, initiating a cycle of flutter while maintaining a constant force. While in these unsteady conditions, an out-of-phase torsional motion is generated where the structure is weakest due to the increased suction, creating this deflection.

	Baseline RANS	Baseline URANS @ 0.08675	FSI T0 – at convergence @ 0.024s	FSI T1 - mid deflection @ 0.037	FSI T2 – Max deflection @ 0.0431	FSI T3 – Mid Deflection @ 0.0506	FSI T4 – at convergence @ 0.0556
CL	7.464	8.86	10.27	12.15	13.04	12.01	11.33
CD	1.03	1.255	1.31	1.16	1.17	1.16	1.155
Max Downforce (N)	128	140	115	128	132	138	138.6

Max Drag (N)	8.87	10.33	18.34	18.44	18.6	18.52	18.62
Max Deflection (mm)	N/A	N/A	0.084	0.595	1.13	0.617	0.0685

Table 5: Transient Simulation of 35-35 Ride height

In the results from the FSI simulation in Table 5 of the initial ride height of 35mm of the chassis at the front and 35mm at the rear, there is a similar level of results found between evaluating the unsteady state of the geometry statically and with deflection. This ride height was selected on the vehicle dynamics optimal ride height for the Oxford Brookes Racing team. A similar analysis was made for the selection of ride height range to provide the chosen configuration between 20mm – 40mm for both front and rear altered by 10mm.

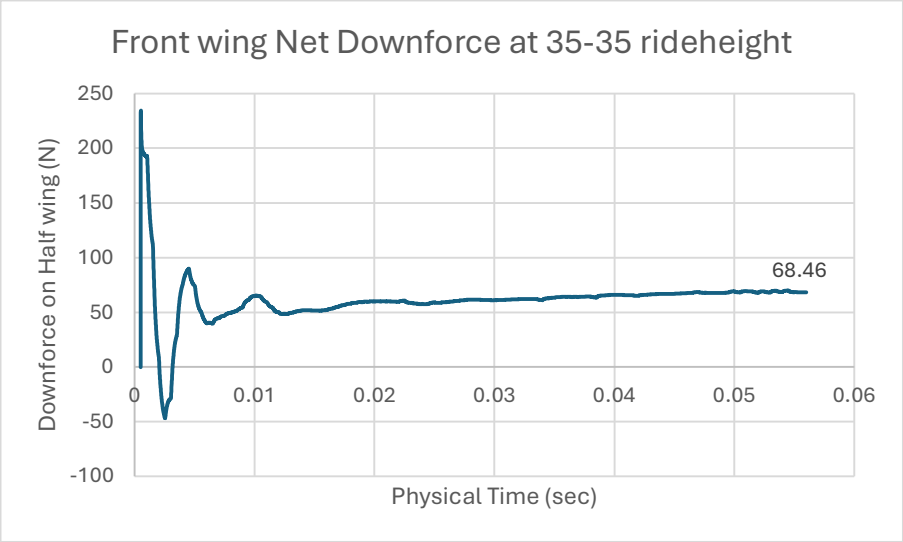

Figure 15: Front wing Net Downforce on Half of FS Full Front wing at 35-35 ride height

In Figure 17, the CP distribution across the airfoil illustrates the downside of taking the net force result of the front wing. This shows that for a given section, different areas on the wing surface may experience greater deflection; however, since the structure is not uniform, it will depend on the response of the structure to this given CP fluctuation.

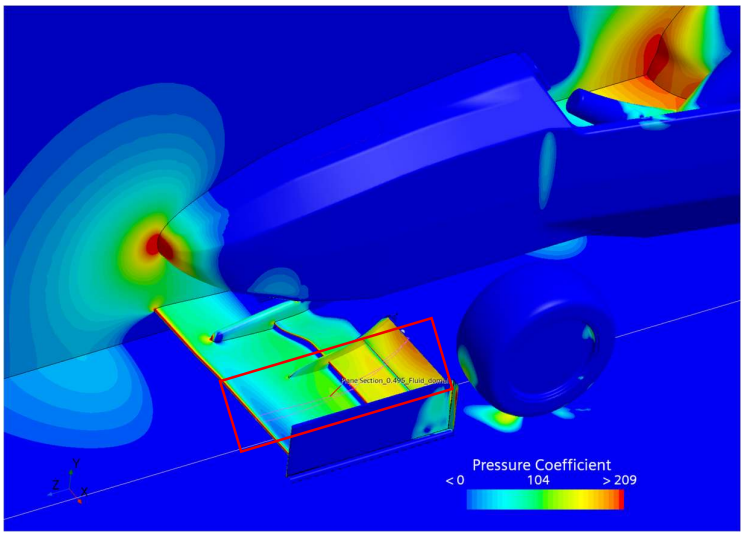

Figure 16: Pressure Distribution cross section of 35-35 FS Front wing at T2

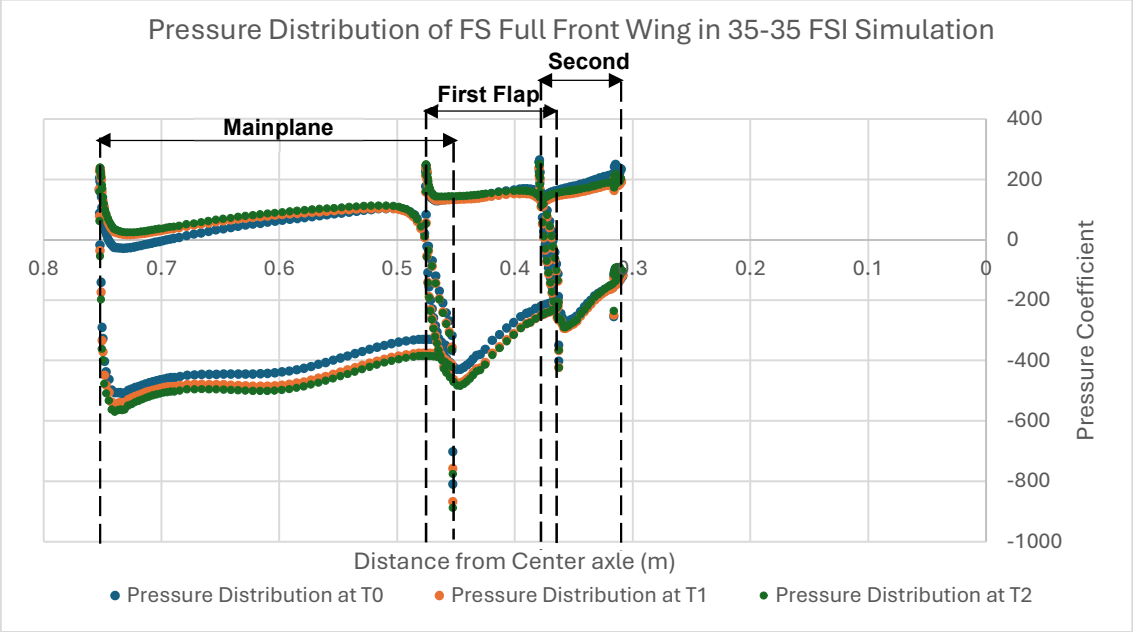

Figure 17: 35-35 Front wing deflection at T2 0.495m from the centre of the vehicle

For this instance, it was taken from an area where the deflection and pressure are highest towards the end of the wings' span, which was 0.495m from the centre of the vehicle, as seen in Figure 16. As there is a variable distribution of the Pressure coefficient from the leading edge to the trailing edge, with an increase in pressure differential with time. This illustration of varying CP in Figure 17 shows that taking the average net downforce of the front wing will not describe the impact on deflection at different areas of the aerodynamic device. By taking the net force and not considering the likely changes in the flaps themselves, coupled with the low damping, the elastic properties of the fluttering wing provide an explanation as to the reason for the downforce remaining relatively consistent when the deflection is still changing over the duration of the short simulation.

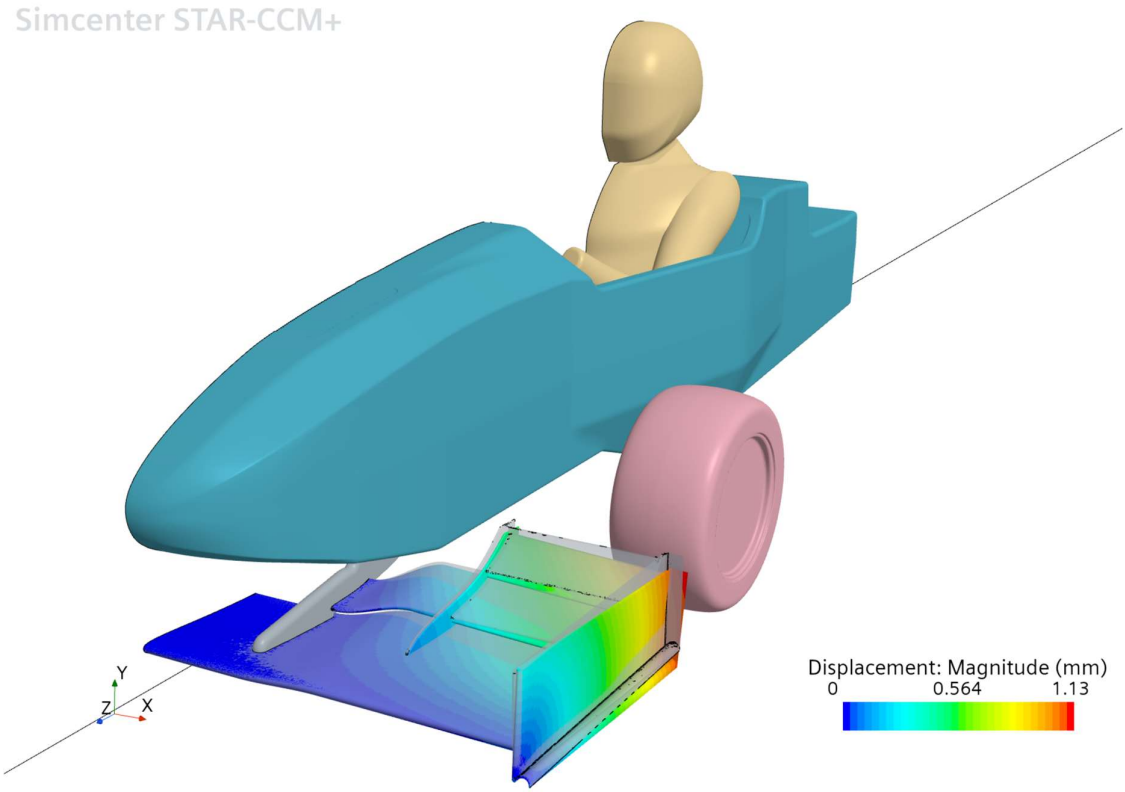

Figure 18: 30-30 Front wing deflection at T2 with a 30% scaled-up deflection representation

During the deflection period, while experiencing increased levels of displacement as seen in Figure 18 the deflection then drops after T2 while the downforce is maintained following the convergence at T0. Ordinarily, the loss of the deflection would be akin to the separation of flow attachment. However, since the load remains consistent, this is a result of the coupled flow changing with time, along with some other factors. A similar level of deflection is found with the varying ride height of the front wing, illustrating the inherent structural effects of this design as it approaches T2 following the convergence of a constant load. With each ride height in the following aero map, the various loads performed similar levels of maximum allowable deflection within similar time intervals for the various heights between T0-T2 and T2-T4. Furthermore, the results of this FSI shows that the downforce of the wing is within 2% of the standard URANS CFD in the 35-35 configuration at a similar timeframe during the unsteady simulation. This provides sufficient correlation between an FSI and non-FSI simulation, further supporting the theory that the structure, combined with the coupled unsteady flow, has a worse reflection of the displacement of different flaps over the general recorded net applied load on the device.

Formula Student Full wing FSI Aero Map

T2 – Max Deflection

		FRH		
		20	30	40
RRH	20	0.837	1.104	0.967
	30	1.234	1.135	1.075
	40	1.283	1.186	1.08

Table 6: Max Deflection for all ride heights

T2 – Max Downforce

		FRH		
		20	30	40
RRH	20	128.0	127.8	126.0
	30	160.3	134.6	121.7
	40	172.2	143.5	130.0

Table 7: Max Downforce for all Ride heights

T2 – Max CLA and CDA

		FRH		
		20	30	40
RRH	20	7.417	7.403	7.301
	30	9.290	7.800	7.051
	40	9.978	8.313	7.533

Table 8: Max Coefficient of Lift for all ride heights

		FRH		
		20	30	40
RRH	20	0.905	1.047	1.263
	30	1.201	1.091	1.124
	40	1.259	1.136	1.050

Table 9: Max Coefficient of Drag for all ride heights

In the aero map results shown in Table 6-9, the optimum performance is illustrated as the vehicle pitches forward. While this analysis only focuses on the analysis of one quarter of the car this information does illustrate how the geometry changes with different static configurations. While the pitching configurations do improve the wing downforce and CLA states, this also increases the amount of deflection and creates greater drag by the changing wake field shown in Table 9. The deflection of the front wing does have an of improvement with the overall net load, as seen in Table 6 between T0 to T2, where there is a greater level of improvement when adjusting the ride height for pitching. In pitching, the wing helps counter the pivot of the wing when deflecting, as seen in Figure 21 below, caused by the suction in the presence of the ground effect not as effective in the other ride heights.

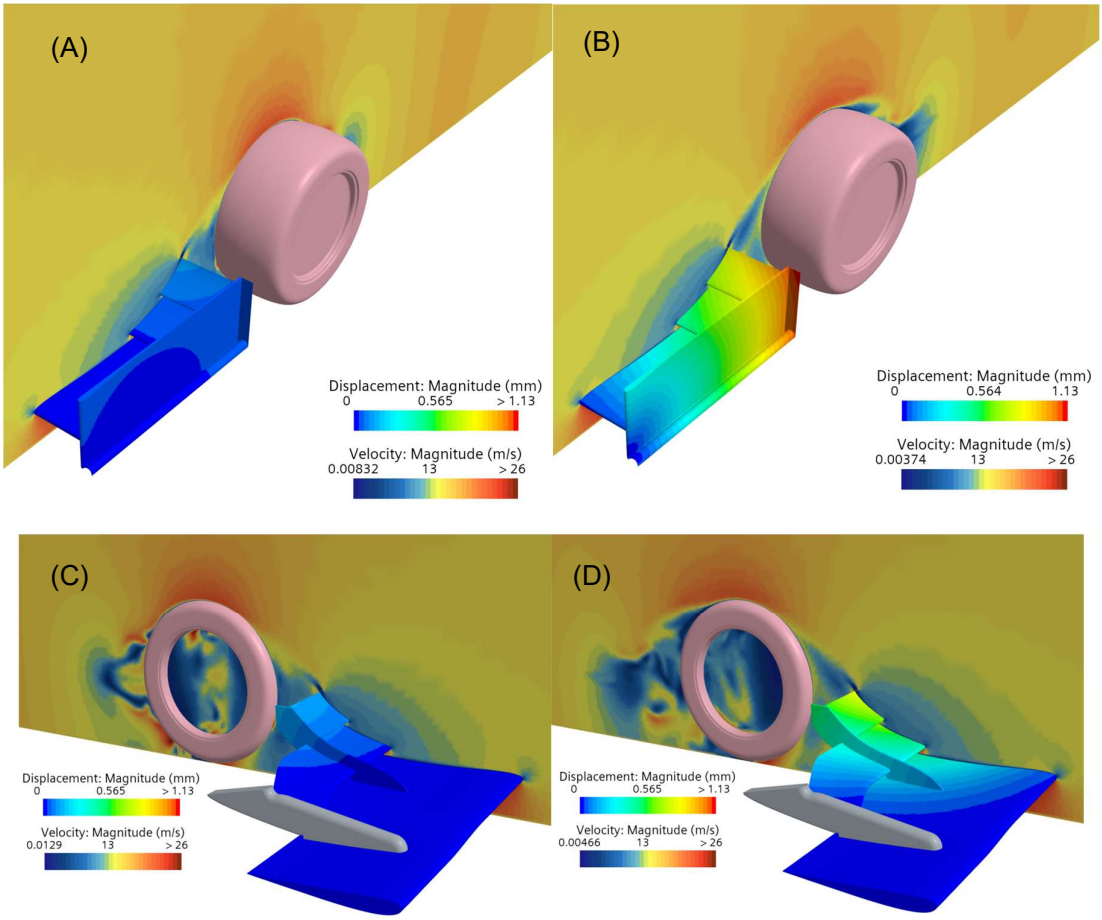

Figure 19: 30-30 Velocity section plane 0.55m from the centre and Deflection on the surface of the wing at (A)Outside view @ T0, (B)Outside view @ T2, (C) Inside view @ T0 & (D) Inside view @ T2

As illustrated in Figure 19, the deflection is minimal with low aerodynamic load at T0 and at peak aerodynamic load at T2. What is also recognised is that the migration of the maximum deflection starts with the upper flaps, then continues to deflect more towards the endplates, illustrating the change in the wing's performance and the benefit of seeing the wing transform in transient simulations.

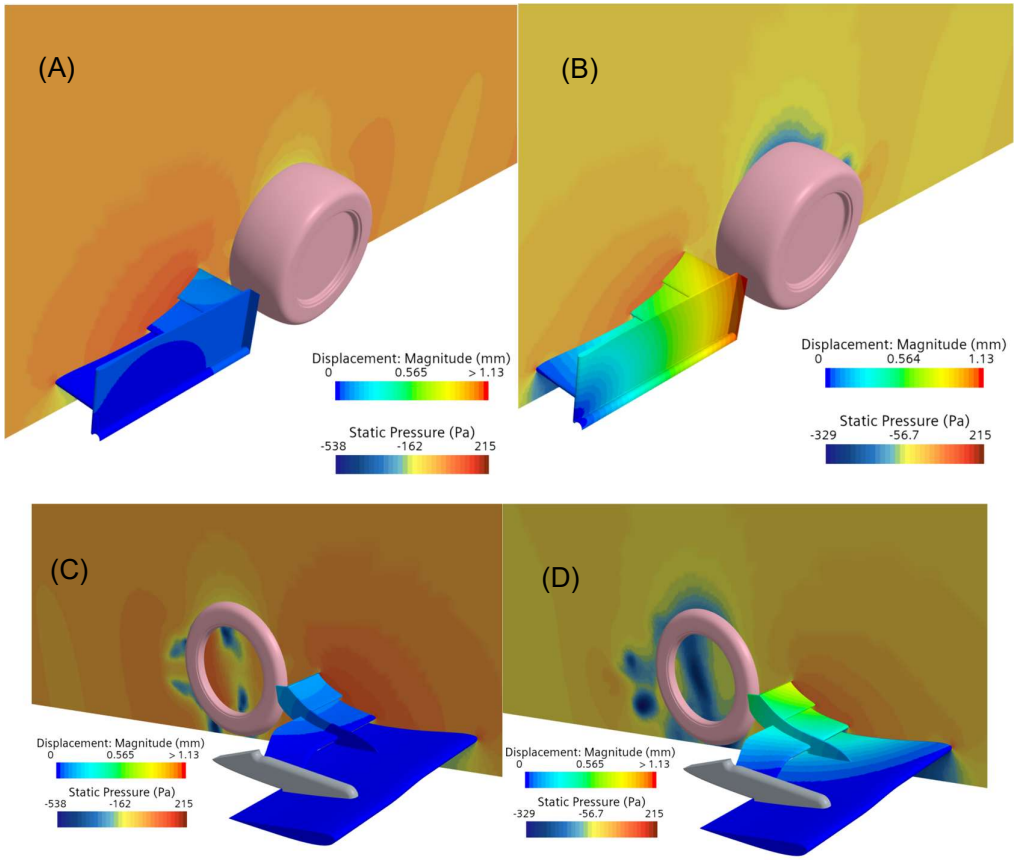

Figure 20: 30-30 Pressure section 0.55m from the centre and Deflection on wing at (A)Outside view @ T0, (B)Outside view @ T2, (C) Inside view @ T0 & (D) Inside view @ T2

The level of deflection in each of the figures above presents a difference in deflection of about 1mm; however, when compared with different time intervals, it illustrates the impact from the pressure distribution once the flow is fully developed over the front wing surface. This progression of the ground effect caused by the wing's deflection, increasing the CP magnitude, is also visible in the transient plot in Figure 17. While there isn't much difference between the force loads between the two intervals compared to the aero map analysis. The pressure in Figures 17 & 20 is still evident, indicating the changes of local surface pressure and showing an impact on the deflection of the upper flaps where the maximum deflection is located.

Discussion

In these results, analysing the Fluid Structure Interaction of the Formula Student Front wing, the analysis shows the impact of not only the benefit of simulating transient fluid flow simulations, but also by seeing the changes in vortices induced by the front wing's outwash. Simulating with this active geometry illustrates the transient response of the wing's load performance as a result of its deflection. The Oxford Brookes Racing load test shows compliance of the tested structure of the wing with the applied 200N load to achieve 2mm of displacement. By referencing this rate of deflection from the deflection test in the highest deflection scenario of 20-40, which produces 172N, the target deflection, therefore, should only be 1.72mm. During this simulation analysis, at no point does the deflection exceed this target, with the highest level of deflection in the 20-40 ride height configuration, achieving a deflection of 1.28mm. This indicates a sufficient level of compliance and correlation with the simulation loads, less than the 200N load and the maximum under the same configuration of 172.2N. These meet the targets set by the physical deflection testing performed by Oxford Brookes Racing and the initial standard CFD simulations of the front wing. There is sufficient

validation to support this methodology for the use of future design iterations, successfully achieving compliant and relatively accurate results. With a longer simulation time, the natural material fatigue resistance of the Carbon fibre would continue to oscillate, but eventually converge on a single displacement.

Changes in the wing's position between 1mm(+/-0.2mm) in this brief FSI simulation duration doesn't have as much change in the wing's performance as with modifying the ride height. The highest performing configuration in transient only increased by 28.7N in deflection. However, by pitching the front axle down and rear axle up by 10mm from 30-30 to the 20-40 configuration resulted in an increase of 36N. It is with these changes that the consideration can be made into how a design will not only perform better in different configurations but also how it will change over time in a given configuration without additional modifications.

Conclusion

In this exploration of simulating a design to illustrate the combined application of Fluid and Structural analysis, an approach was developed. The experimentation of this material for a given design shows that changing the wing structure provides different levels of performance to benefit the versatility of the car. While other traditional methods were explored first in this study, the change in performance with the added structural interaction shows there is a gap between standard CFD methodology. By first illustrating the benefits of the use of Unsteady over steady state conditions, to then producing a baseline FSI template to evaluate in an aero map, was used to explore the versatility of the design. This research provides avenues for further investigation into applications of transient simulations for an improved level of fluid dynamic representation, accurate to real-world performance.

While this structural design analysis is applicable to other aerodynamic devices for improving the vehicle's performance. The study has shown large levels of improvement with the benefit of the deflection from ground effect suction, which is not present in many other aerodynamic device applications.

Therefore, by relying on the elastic properties of the wing's structure, there are avenues to pursue material design benefiting levels of deflection in given parts of track performance. In exploring the material and fluid analysis prevents compromising the vehicle dynamics of a performance car by not solely relying on the vehicle kinematics for aerodynamic performance. Providing further development to this study with longer simulation times to illustrate the settled displacement where the wing has converged and with accurate laminate specification, would be the next steps for future applications of this validation method. This concurrent simulation method holds great potential for illustrating and developing improved performance through the accurate combination of structural design and fluid mechanics analysis.

References

Fuentes, D., Cura Hochbaum, A. and Schulze, R. (2023) “Numerical and experimental fluid–structure interaction analysis of a flexible propeller,” Ship Technology Research, 70(3), pp. 163–173. Available at: https://doi.org/10.1080/09377255.2022.2115241.

Ntoukas, G. et al. (2025) “A comparative study of explicit and implicit Large Eddy simulations using a high-order discontinuous Galerkin solver: Application to a Formula 1 front wing,” Results in Engineering, 25, p. 104425. Available at: https://doi.org/10.1016/j.rineng.2025.104425.

Bang, C.S. et al. (2022) “Numerical Investigation and Fluid-Structure Interaction (FSI) Analysis on a Double-Element Simplified Formula One (F1) Composite Wing in the Presence of Ground Effect,” Fluids, 7(2), p. 85. Available at: https://doi.org/10.3390/fluids7020085.

Yuanjing Wang et al. (2023) “Study on Fluid-Structure Interaction of a Camber Morphing Wing,” Vibration, 6(4), pp. 1060–1074. Available at: https://doi.org/10.3390/vibration6040062.

Ghaedi, K. et al. (eds.) (2021) Computational overview of fluid structure interaction. London: IntechOpen. Available at: http://search.ebscohost.com/login.aspx?direct=true&site=edspub-live&scope=site&type=44&db=edspub&authtype=ip,guest&custid=ns011247&groupid=main&profile=eds&bquery=AN%2030082938 (Accessed: February 28, 2025).

Brockmeyer, L. et al. (2024) “Evaluation of RANS vs. LES simulation of fluid flow through 3 × 3 rod bundle with a simple spacer grid as a precursor to coupled fluid-structure interaction simulations,” Nuclear Engineering and Design, 430. Available at: https://doi.org/10.1016/j.nucengdes.2024.113662.

Mattia Basso, Carlo Cravero and Davide Marsano (2021) “Aerodynamic Effect of the Gurney Flap on the Front Wing of a F1 Car and Flow Interactions with Car Components,” Energies, 14(8), p. 2059. Available at: https://doi.org/10.3390/en14082059.

Zhang, G. et al. (2024) “Aerodynamic Design and Performance Research of Racing Cars with Adaptive Control of Attitude,” International Journal of Automotive Technology, 25(4), pp. 901–912. Available at: https://doi.org/10.1007/s12239-024-00056-0.

Patil, S. et al. (2015) “Fluid Structure Interaction Simulations Applied to Automotive Aerodynamics,” SAE Technical Paper [Preprint]. Available at: https://doi.org/10.4271/2015-01-1544.

Ratzel, M. and Dias (2014). Fluid - Structure Interaction Analysis and Optimization of an Automotive Component. SAE International.

Jaiman, R., Thomas, H. and Shakib, F. (2012) Direct-Coupled Fluid-Structure Interaction for Automotive Applications. SAE International.

Marco Gadola et al. (2022) “Analyzing Porpoising on High Downforce Race Cars: Causes and Possible Setup Adjustments to Avoid It,” Energies, 15(18), p. 6677. Available at: https://doi.org/10.3390/en15186677.

Roberts, L.S. et al. (2016) “Aerodynamic characteristics of a wing-and-flap configuration in ground effect and yaw,” Proceedings of the Institution of Mechanical Engineers, Part D: Journal of Automobile Engineering, 230(6), pp. 841–854. Available at: https://doi.org/10.1177/0954407015596274.

Khayyer, A. et al. (2022) “A 3D SPH-based entirely Lagrangian meshfree hydroelastic FSI solver for anisotropic composite structures,” Applied Mathematical Modelling, 112, pp. 560–613. Available at: https://doi.org/10.1016/j.apm.2022.07.031.

Rangarajan, K. et al. (2025) “Numerical Study of Aerodynamic Flow and the Effects of Spoiler Wings on a Formula Student Race Car,” SAE Technical Paper [Preprint]. Available at: https://doi.org/10.4271/2024-01-5247.

Karthikeyan, P.N., Radhakrishnan, J. and Automotive Technical Papers Warrendale, Pennsylvania, United States 2024-01-01 (2024) “Optimizing High-Lift Airfoils for Formula Student Vehicles,” SAE Technical Paper [Preprint]. Available at: https://doi.org/10.4271/2024-01-5059.

OBR25 25-AE-110 “Front Wing MAR” Design Report. Available at: https://docs.google.com/document/d/1Q0w7a2vXQI_lGXbg6UGJP4zhW55-r5mJ/edit?usp=sharing&ouid=110705055988163397923&rtpof=true&sd=true

Wilcox, D.C. (2008) ‘Formulation of the k-ω turbulence model revisited’, AIAA Journal, 46(11), pp. 2823–2838. Available at: https://2024.sci-hub.se/7105/07e48dc0ee4aa8a5f77f0c83edd1be18/wilcox2008.pdf

OBR25 Front Wing Design Timeline. Available at: https://drive.google.com/file/d/1vALJMcGpnlVoGPa00acz-q3qEuuJmf2B/view?usp=sharing

OBR24 Tensile testing GG245T 3k 3plys (45,090,45). Available at: https://drive.google.com/file/d/159mQHmz3XJN-yGOb0jub3-41OmXashTp/view?usp=drive_link

Gong, Y. & Zhang, W., 2019. Efficient Aeroelastic Solution Based on Time-Spectral Fluid-Structure Interaction Method. AIAA Journal, 57(7), pp.3014-3025

Appendices

Additional Formulae

$$\frac{\partial}{\partial t}(\rho k) + \frac{\partial}{\partial x_j}(\rho u_j k) = \rho \tau_{ij} \frac{\partial u_i}{\partial x_j} - \beta^* \rho k \omega + \frac{\partial}{\partial x_j}\left[\left(\mu + \sigma^* \frac{\rho k}{\omega}\right)\frac{\partial k}{\partial x_j}\right] \quad (1)$$

$$\frac{\partial}{\partial t}(\rho \omega) + \frac{\partial}{\partial x_j}(\rho u_j \omega) = \alpha \frac{\omega}{k} \rho \tau_{ij} \frac{\partial u_i}{\partial x_j} - \beta \rho \omega^2 + \sigma_d \frac{\rho}{\omega} \frac{\partial k}{\partial x_j} \frac{\partial \omega}{\partial x_j} + \frac{\partial}{\partial x_j}\left[\left(\mu + \sigma \frac{\rho k}{\omega}\right)\frac{\partial \omega}{\partial x_j}\right] \quad (2)$$

Acknowledgement

I am deeply grateful to all those who have aided in this study. There are those whose resources and insight have been very beneficial in helping accomplish the extent of this research and are worth recognising.

I would like to firstly thank Oxford Brookes Racing for using the design and materials for my Fluid Structure Interaction study. Without these resources, much of the time spent during this research would have been otherwise dedicated to design and less towards the exploration in validation.

The computational equipment used in this research was crucial to exploring this validation, which could not have been accessible without Oxford Brookes University and Oxford Brookes Racing.

Finally, with the assistance and guidance of Dr Edward Hopkins, of Oxford Brookes University's School of Engineering, Computing and Mathematics, for providing a new and different level of computational analysis and the next level of experimentation in Fluid Dynamics.

While there has been a provision in place for minimal resources to explore the topic of this research. Without these acknowledged assets, the conclusion would not have been supported by nearly as many or as accurate findings.